Metals

CrossMark

Effects of pre-recovery on the recrystallization microstructure and texture of high-purity tantalum

S. F. Liu[1,*], Y. H. Liu[1], L. J. Li[1], C. Deng[1], H. Y. Fan[1], Y. Guo[1], L. F. Cao[1], and Q. Liu[1,*]

[1] College of Materials Science and Engineering, Chongqing University, Chongqing 400044, China

ABSTRACT

The effects of recovery on the subsequent recrystallization of tantalum were investigated via two-step annealing at two temperatures. Transmission electron microscopy, electron back-scattered diffraction, and X-ray diffraction were employed to determine the respective microstructures and textures after various annealing regimes. The results show that many large grains with {111} <uvw> orientations are developed when heating at 1573 K without pre-recovery, while pre-recovery can introduce a homogeneous fine microstructure and weaken the texture. This difference can be attributed to the recovery-induced change in nucleation mechanisms. Elongated grains stretch along grain boundaries or locate in the interior of deformed grains, mainly due to the heterogeneous distribution of stored energy. Dislocations characterized by submicron bands in the deformed state evolve into sub-grains during pre-recovery and grow continuously, indicating a homogeneous distribution of dislocation or stored energy after pre-recovery, which can significantly influence subsequent nucleation and grain growth.

Introduction

Most deformation energy evaporates during cold working, and only a very small fraction ($\sim 1\%$) remains in the material as defects [1–3]. Stored energy usually serves as a driving force for some non-equilibrium transformation behaviors, such as recovery, recrystallization, and grain growth [4, 5]. Recovery, which is a thermally activated process generally occurring at relatively low temperatures, plays a key role in reinstating various properties and parameters, especially the restoration of microstructure [6]. Theoretically, unlike dramatic changes

during recrystallization, recovery primarily influences the nucleation and dislocation activities within distorted grains, without any grain boundary migration [7]. Primary recrystallization mostly refers to the occurrence of strain-free grains and subsequent growth [1]. The interaction between recovery and recrystallization is an ongoing research topic, and the benefits of clarifying this interaction, e.g., controlling and designing material performance, deserve deep investigation [8]. Recovery, for example, promotes the formation of R texture in an Al–Mg alloy but restrains the cube texture, as investigated by Liu et al. [9], thus tailoring the anisotropy of properties. Some

Springer

computer-aided simulations also verify such an interrelationship between recovery and recrystallization. For instance, a physical-based model shows that pre-recovery would limit the recrystallization of materials with low stacking-fault energy (SFE), while the opposite is observed for high-SFE metals [8]. A recent study of Nb [10] indicates that numerous subgrains serving as nuclei for recrystallization stem from {111} oriented grains (i.e., <111> parallel to the normal direction (ND)) when deformed structures undergo a substantial recovery, thus accelerating the recrystallization process.

Fine grains with uniform orientations are of great concern when fabricating sputtering targets [11]. Given the huge influence of texture and microstructure on the sputtering performance and quality of films, revealing the mutual effects between recovery and recrystallization is particularly important for tantalum (Ta) sputtering targets. However, the annealing behavior of Ta has not drawn the same attention and efforts as some well-known metallic materials. Our recent quantitative studies show that the stored energy in Ta largely varies with grain orientation [12]. Therefore, recovery may have strong orientation-dependent effects on the recrystallization behavior of Ta, which has not yet been fully understood. It is therefore the aim of this work to investigate the effects of pre-recovery systematically. In light of the positive roles in optimizing the texture and microstructure of Ta [13], clock rolling, in which the rolling direction is sequentially changed by 135° about the ND, is adopted in this study. Meanwhile, multi-scale characterization techniques and analytical procedures are used to reveal the microstructure and texture evolution in Ta.

Experiments

A tantalum plate with 87% thickness reduction was obtained by 135° clock rolling, and several specimens ($10^L \times 8^W \times 3^T$ mm^3) were cut from the plate adjacently. The chemical composition and rolling parameters are shown elsewhere [13]. Low-temperature annealing (LTA) at 1073 K for 0, 5, 10, 30, and 60 min, followed by high-temperature annealing at 1573 K for 60 min (HT-60), was imposed on all samples (hereafter referred to as R1, R2, R3, R4, and R5, respectively, as shown in Table 1). An inert

Table 1 Details of annealing regimes for specimens

Specimens	R1	R2	R3	R4	R5
LTA (1073 K) (min)	0	5	10	30	60
HT-60 (1573 K) (min)	60	60	60	60	60

atmosphere was used for resistance to high-temperature oxidation.

The center region of the ND-RD (rolling direction) plane was characterized using a high-speed electron backscatter diffraction (EBSD) detector attached to a scanning electron microscope (SEM, Tescan Mira 3). Specimens were prepared by fine mechanical polishing followed by electro-polishing using a mixture of hydrofluoric acid and sulfuric acid (1:9 by volume) at ambient temperature. EBSD measurements were conducted at an accelerating voltage of 20 kV. Here, the grains were classified into the following three groups based on their orientations: {111} <uvw> (<111>//ND) grains, {100} <uvw> (<100>//ND) grains, and the "random" group which refers to any other grains except for {111} <uvw> and {100} <uvw> grains. The tolerance to define the texture components was 15°.

The substructures of the as-rolled specimen and those annealed at 1073 K for various times were checked using a transmission electron microscope (TEM, JEOL 2100). All specimens (3 mm in thickness) were taken from the ND-RD section and jet-polished in a mixture of hydrofluoric acid, sulfuric acid, and methyl alcohol (1:5:94 by volume) at 273 K. The operating accelerating voltage was 200 kV.

The macro-texture information was acquired from the mid-layer of the RD-TD (transverse direction) plane using an X-ray diffractometer (XRD, Rigaku D/max 2500 PC) with Cu Kα radiation. Four pole figures, (110), (200), (211), and (222), were recorded up to a maximum tilt angle of 70°. The arbitrarily defined cells (ADC) method was used to calculate orientation distribution functions (ODFs) from the above pole figures, and Labo Tex 3.0 software was used for quantitative analysis of texture.

Results

Recrystallized microstructures for specimens with various annealing conditions are shown in Fig. 1. The highly developed recrystallization microstructure can
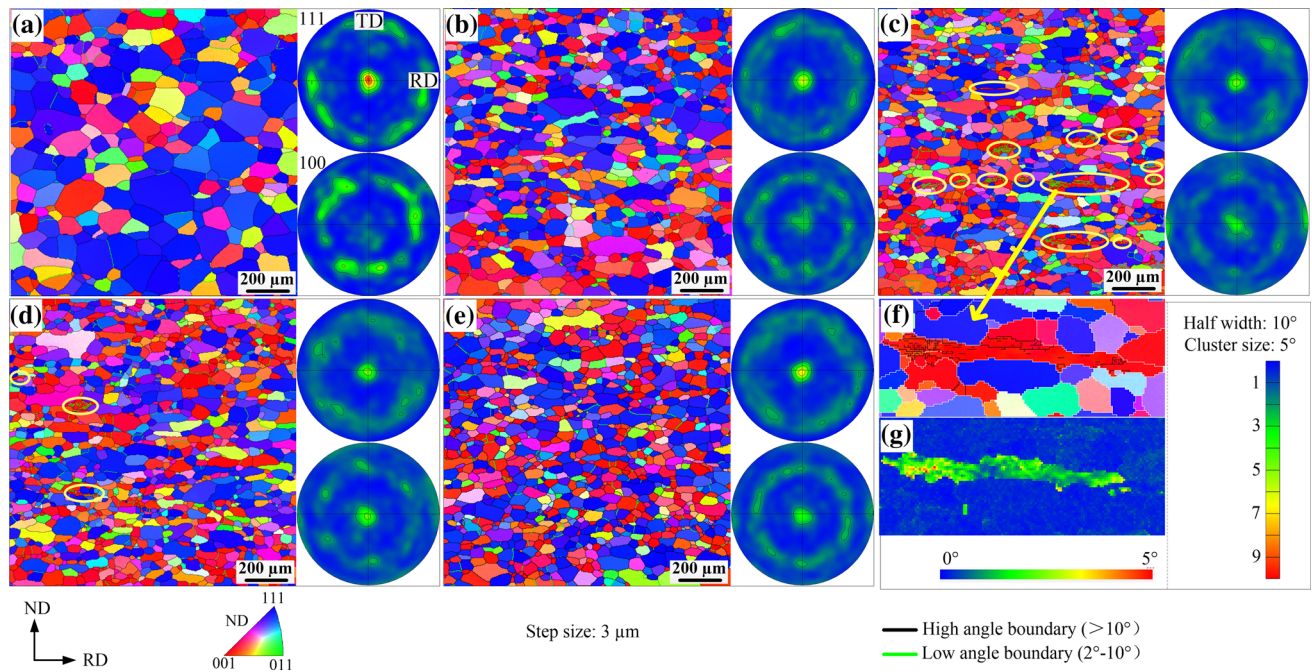
Figure 1 Microstructure evolution for specimens under various annealing conditions. **a** R1, **b** R2, **c** R3, **d** R4, and **e** R5; **f** and **g** are regions containing un-recrystallized substructures in Fig. 1c.

be seen in the R1 and R2 specimens, as shown in Fig. 1a and b. R3 and R4 still remain some distorted structure wrapped by low-angle boundaries (as marked by ellipses in Fig. 1c, d), with the degree of recrystallization was 93.0 and 94.3%, respectively. Most of the residual deformation blocks are in {100} orientations. As shown in Fig. 1f and g, the region containing un-recrystallized substructures is extracted from Fig. 1c. Additionally, the keranel average misorientation (KAM) clearly reveals these distorted substructures in Fig. 1g. A fully recrystallized structure with a smaller grain size is shown in the R5 specimen (Fig. 1e), and therefore, we regard the annealing schedule for R5 as the best configuration in this paper. Corresponding pole figures show grains densely distributed in the <111> direction in the R1 and R2 samples, but the density declines sharply in R3 and R4. It appears that grains have much more random orientations after LTA treatment.

Figure 2a shows the plot of the average size of recrystallization grains versus LTA time. More specifically, the equal-area method equipped in Channel 5 software is employed to determine the grain size. Grain size is obviously influenced by the recovery level. As LTA proceeds, the average grain size decreases sharply during the first 10 min and

then increases slightly. Which recrystallization grains are considered eligible should be defined for incompletely recrystallized samples, e.g., R3 and R4. Given Ref. [14] and the identification limit of the EBSD technique, grains with sufficiently small intra-granular orientation gradients ($< 1°$) and sufficiently large sizes (> 10 μm) are extracted from specimens R3 and R4. As presented in Fig. 2b, the average grain size shows a prominent orientation dependence: The {111} grains are obviously larger than others, especially the smallest {100} grains.

Recovery influences not only the grain size but also the grain morphology. Here, we use aspect ratio maps (Fig. 3) to show the grain shape evolution with annealing time. While R2, R3, and R4 have more or less elongated grains that are green or even red, it is glaring that almost all grains in the R5 specimen are blue, indicating an equiaxed structure. Elongated grains, including the residual deformed bands, are mostly red and roughly parallel to the rolling direction.

The annealing texture from X-ray analysis is shown in Fig. 4. Only the primary θ-fiber and γ-fiber texture are considered in this study. The textures {001} <100> and {001} <110> are two dominant components in the θ-fiber (ND//<100>), and the γ-
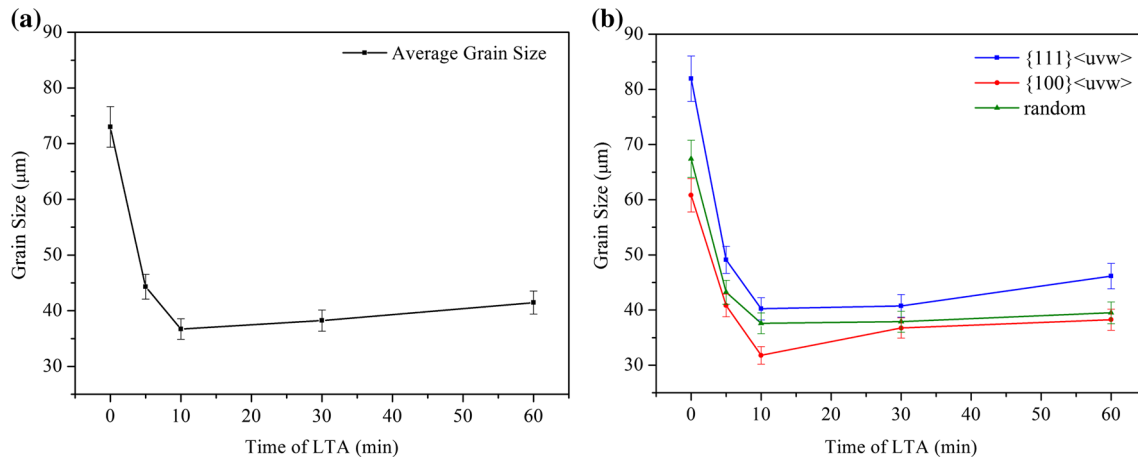
Figure 2 Evolution of grain size with low-temperature annealing (LTA); **a** average recrystallization grain (RG) size versus LTA time and **b** size of differently oriented RGs versus LTA time.
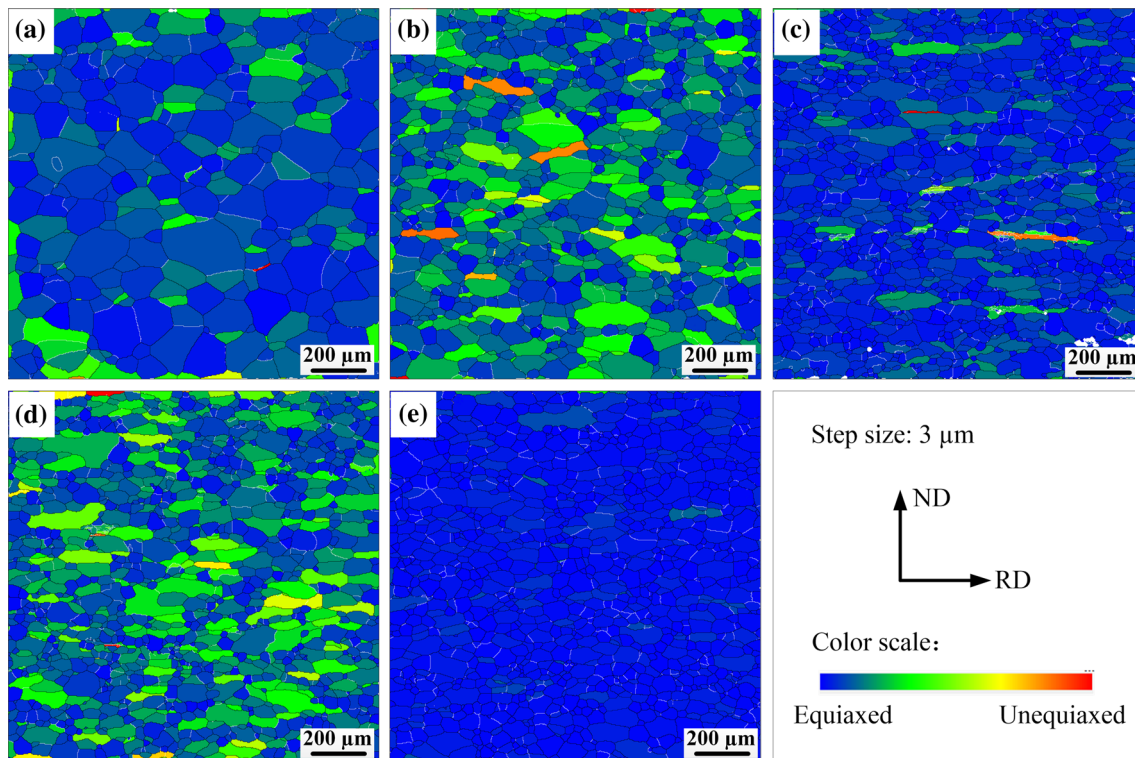

Figure 3 Aspect ratio maps of samples: **a** R1, **b** R2, **c** R3, **d** R4, and **e** R5.

fiber (ND//<111>) mainly contains {111} <011> and {111} <112>. Detailed definitions of the two fibers are shown elsewhere [13]. The R1 specimen exhibits a strong γ-fiber, more specifically the {111} <112> texture, showing a good match with the pole figure (Fig. 1a). However, the γ-fiber is weakened, and the θ-fiber is significantly enhanced for R3 and R4.

The respective evolutions of the γ-fiber, θ-fiber, and other orientations with LTA are depicted quantitatively in Fig. 5. For R1, the γ-fiber occupies approximately 57% of the total and the θ-fiber only 8%. The intensity of the γ-fiber decreases, while that of the θ-fiber increases after a 5-min LTA. Compared to R1 and R2, the γ-fiber decreases remarkably in R3, while
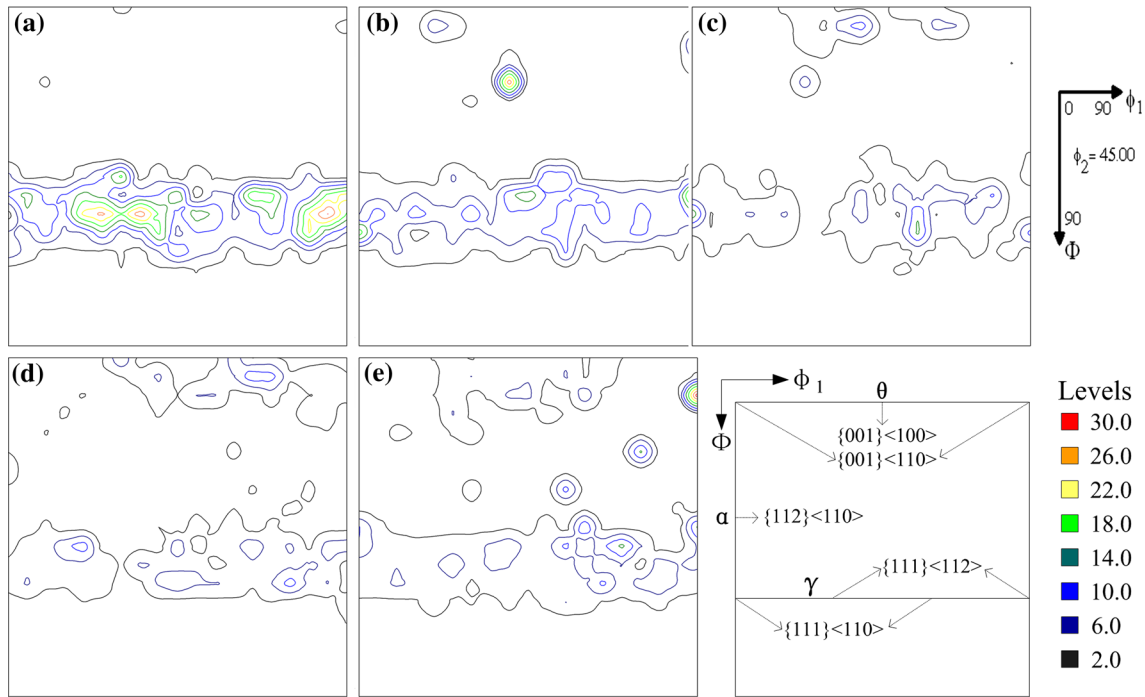
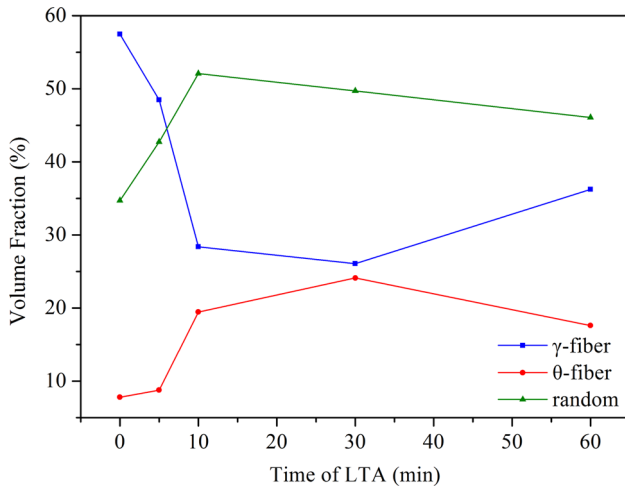**Figure 4** ODF sections. **a** R1, **b** R2, **c** R3, **d** R4, and **e** R5.

Figure 5 Respective evolution of γ-fiber, θ-fiber, and other orientations.

the θ-fiber increases dramatically. A similar but more moderate tendency of the two fibers was then observed with continuous pre-recovery (30 min). For further annealing [60 min (R5)], the γ-fiber intensity increases somewhat, but the θ-fiber decreases continuously. In the R5 specimen, γ-fiber grains account for 36% of the total; for the θ-fiber, the amount is 18%.

Discussion

Recovery-dependent nucleation

Various structures are visible in annealed specimens without HT-60. The annihilation and rearrangement of dislocations and the vanishing of point defects during recovery could greatly reduce the magnitude and tailor the distribution of stored energy in materials and can thus affect the nucleation of recrystallization. Nucleation is generally activated via the growth of sub-grains or the migration of high-angle boundaries (HABs). HABs migrate rapidly at high temperatures and sweep the deformation substructures induced from cold working; at low temperatures, sub-grains grow to develop new mobile HABs [1, 4]. Sub-grain boundaries mostly exhibit low angles, and the accumulation of higher misorientation requires local orientation gradients around these sub-grains [4, 15]. More specifically, sub-grain growth (SG) can be further divided into two parts: sub-grain coarseness and sub-grain coalescence. The former means that sub-grains grow rapidly into a recrystallization nucleus by discontinuous or abnormal growth, while the latter means that sub-grains rotate by boundary diffusion processes until adjacent sub-grains have similar orientations and coalesce into

a large sub-grain. Compared to the nucleation mechanism of high-angle boundary migration (HABM), SG is an extremely sluggish procedure and requires sufficient time to form effective nuclei at low temperature [4, 16].

As shown in Table 1, an HT-60 (1573 K, 60 min) following a sequence of LTA treatments was applied, aiming to explore how pre-recovery impacts nucleation behaviors. In this study, 1073 K is selected as a pre-recovery temperature because it is not sufficient to induce extensive recrystallization, as assessed from differential scanning calorimetry (DSC) curves in Ref. [12].

EBSD measurements were performed to ensure that no obvious recrystallization occurs at 1073 K, as presented in Fig. 6. It is easy to identify some well-formed sub-grains (2°–7.5°) in the specimens after 30 and 60 min, as shown in Fig. 6c, d, even though the deformed microstructures are mostly preserved. In addition to the increased number, sub-grains also became plump and larger with time. Furthermore, some sub-grain boundaries evolved gradually into HABs after 60 min under LTA, as illustrated in Fig. 6d. To gain greater insight into substructure morphologies, TEM observations were performed for

the rolled and LTA specimens. Figure 7a shows a part of a γ-fiber grain, in which dislocations evolve into submicron band structures (0.1–0.4 μm in width) surrounded by dislocation walls. Annealing can gradually change the dislocation configuration, along with a transformation from submicron bands to sub-grains. After recovery for 5 min, the submicron bands change somewhat, and the amount of dislocations in the interior of the bands decrease to some extent. After a 10-min recovery (Fig. 7c), dislocation walls appear to narrow significantly, and some coarse sub-grains emerge via sub-grain coalescence. Dislocations within these sub-grains are at the point of annihilation, as shown by red arrows in Fig. 7c, thus coarsening sub-grains to 0.5–1 μm. After 60 min, larger well-developed sub-grains are clearly observed, and dislocations also show a more homogeneous distribution. In particular, sub-grains formed during pre-recovery tend to be equiaxed as shown in Fig. 7e. If some sub-grains exceed a critical size, they can be identified as an effective and thermostable nucleus that can sweep the surrounding deformed structure during subsequent growth [4]. These changes could greatly influence the subsequent recrystallization,

Figure 6 Grain-boundary evolution of specimens under different annealing conditions. **a** At 1073 K for 5 min, **b** at 1073 K for 10 min, **c** at 1073 K for 30 min, and **d** at 1073 K for 60 min.
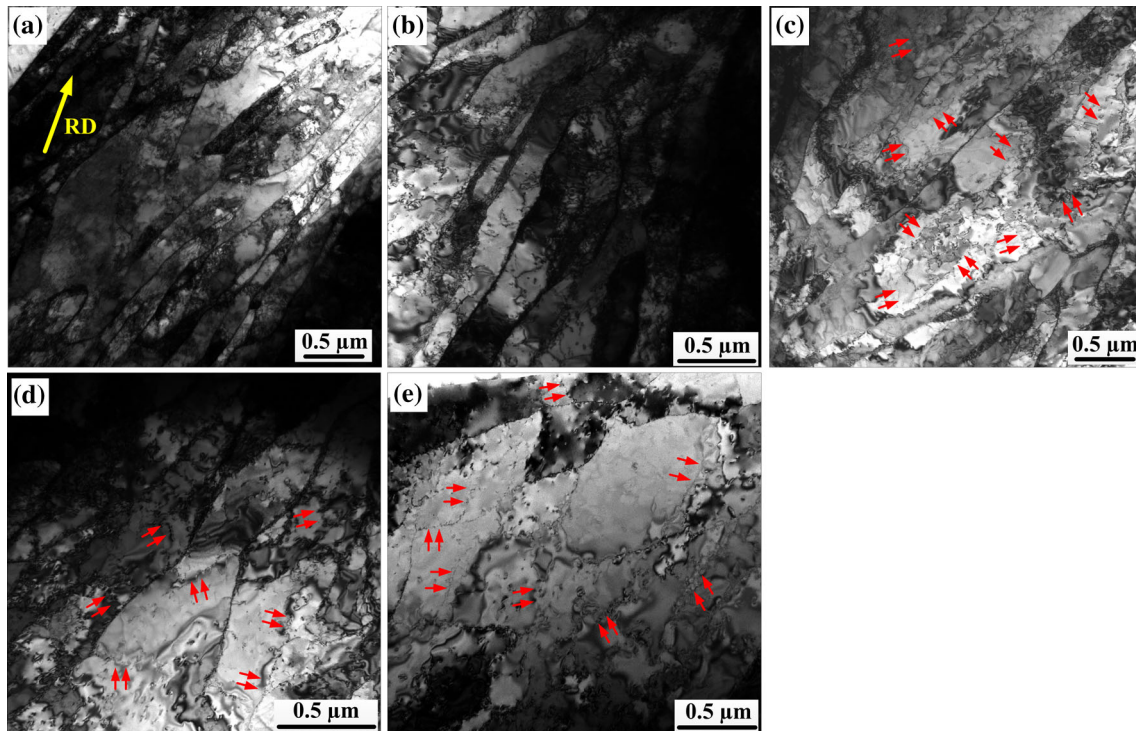

Step size: 0.05 μm   2° 7.5° 10° 20° 30° 40° 50°
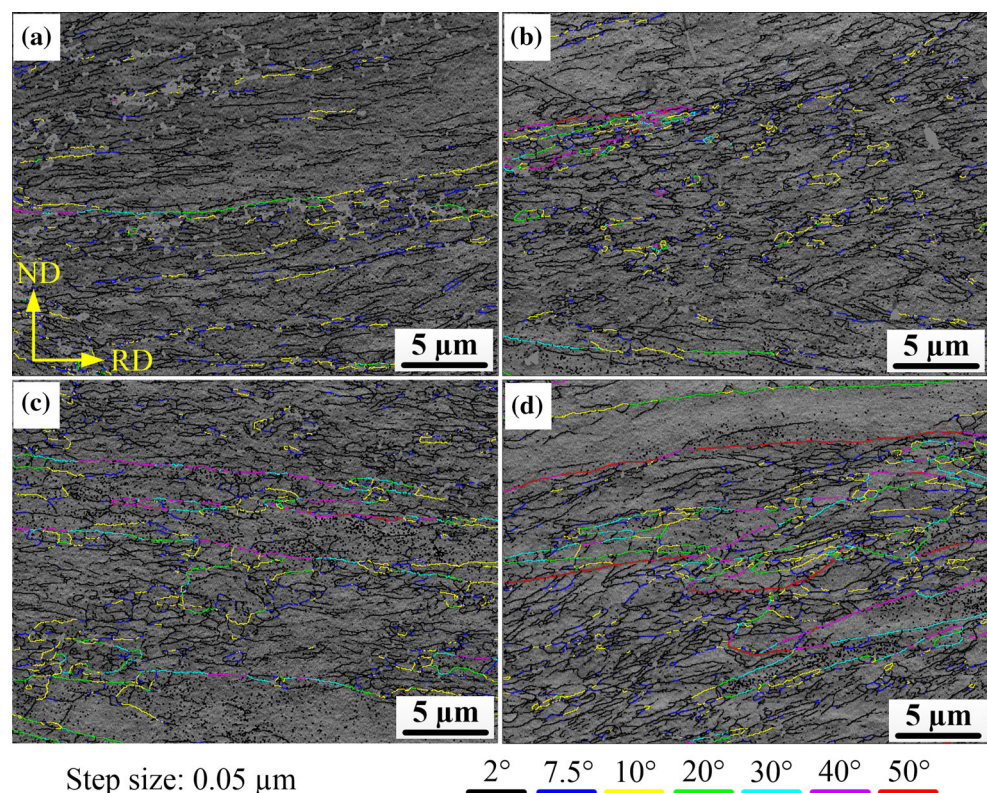
Figure 7 TEM observation of specimens under different conditions. **a** Cold rolling, **b** at 1073 K for 5 min, **c** at 1070 K for 10 min, **d** at 1070 K for 30 min, and **e** at 1073 K for 60 min.

such as grain size, grain shape, and texture evolution, which will be analyzed later.

To capture an intermediate state of recrystallization, all specimens with different levels of pre-recovery were heated at 1573 K for 2 min, resulting in 80.8, 77, 64.9, 62, and 62.4% recrystallization, with different amounts of residual deformation bands attached, as shown in Fig. 8. Note that these bands are mostly in the {100} orientation, as evident from Fig. 8d and e. The corresponding texture evolution is summarized in Fig. 9; the {111} components decrease continuously, whereas the random-oriented ones show an increasing trend. Additionally, the average grain sizes, 28.79, 28.95, 26.06, 27.07, and 27.24 μm, were calculated, indicating that the evolution of the average grain size is a similar but has a more moderate tendency compared with that of specimens after HT-60 annealing (Fig. 2).

Influence of recovery on grain size

The formation of sub-grains is time-dependent, and their growth is energy dependent, causing grain size variations at different annealing periods. The sub-grain formation is mainly associated with the rearrangement of dislocations or the migration of low-angle boundaries, and the migration rate is slow during LTA. As depicted above, the sub-grain number for the R2, R3, R4, and R5 specimens increases successively with LTA time, together with the various degrees of stored energy decreasing successively. Thus, specimens that experienced long-time recovery, e.g., R4 and R5, do not have enough energy to drive the rapid migration of HABs. For Ta, the deformation texture typically contains γ-fiber and θ-fiber orientations, and prominent intra-granular orientation gradients develop readily in γ grains. Studies have reported that γ grains, especially the regions near grain boundaries, are preferential nucleation sites [17–19].

Compared to other specimens, R1 and R2 experienced shorter times for LTA and therefore have higher stored energy; it can be deduced from Figs. 1a, b and 7a, b that the HABM mechanism dominates nucleation in the R1 and R2 specimens. The HABs in R1 and R2, including the {111}–{100} boundaries and HABs forming in the grain interior during rolling, migrate and sweep the deformation substructures rapidly at a high temperature, which leads to larger grains in these two specimens. For the R5 specimen, a
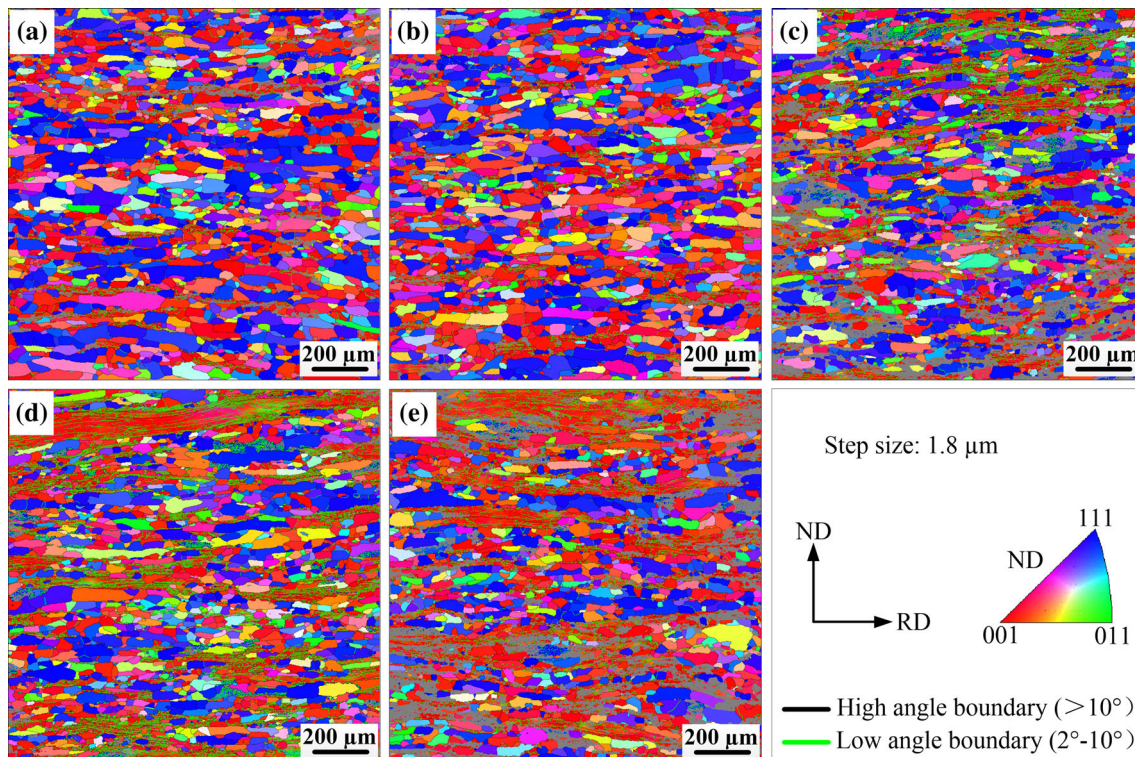
Figure 8 Partially recrystallized specimens experienced various pre-recovery and heating at 1573 K for 2 min; **a** at 1073 K for 0 min before 1573 K for 2 min; **b** at 1073 K for 5 min before 1573 K for 2 min; **c** at 1073 K for 10 min before 1573 K for 2 min; **d** at 1073 K for 30 min before 1573 K for 2 min; and **e** at 1073 K for 60 min before 1573 K for 2 min.
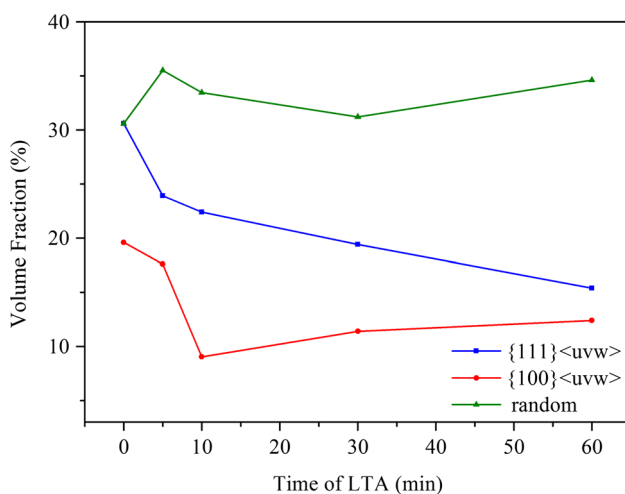

Figure 9 Evolution of different texture components for partly recrystallized specimens.

considerable number of sub-grains dominate the nucleation process, resulting in smaller grains after HT-60 treatment. For the R3 and R4 specimens, the residual deformed structures arose for the following two reasons. Because of the shorter time of LTA, less effective nuclei form via the SG model in the R3 and

R4 specimens compared to R5. In addition, the stored energy in R3 and R4 is less than that in R1 or R2 due to the longer-time LTA. Thus, the driving force to coarsen the nuclei formed during pre-recovery is insufficient. Additionally, {111} grains are consumed by the growing nuclei prior to the {100} grains with lower stored energy.

Influence of recovery on grain shape

The recovery process changes the amount and distribution of dislocations, and these changes are a function of recovery time. Namely, the distribution of stored energy is heterogeneous and time-dependent, which would influence the grain shape during annealing.

For the R1 specimen, the sufficient stored energy introduces adequate growth of the recrystallized grains, and thus, they tend to be equiaxed. Gaitzsch et al. also suggested that high-temperature annealing might cause more equiaxed grains to form in Ni5 W [20]. In R5 specimen, grains also emerged in highly equiaxed shapes, which can be mainly attributed to the fact that there are many equiaxed nuclei formed

by the SG mechanism before recrystallization due to sufficient recovery. In addition, the driving force was nearly exhausted during the long-time LTA, which makes abnormal growth of nuclei impossible. For the R2, R3, and R4 specimens, effective nuclei formed by sub-grains are fewer in number compared to the R5 specimen. In addition, in the R2, R3, and R4 specimens, the driving force difference between the grain boundary and the grain interior is more pronounced than the R5 specimen. Consequently, nuclei that formed in grain boundaries elongated in the grain.

Influence of recovery on texture evolution

There are a few effective recrystallization nuclei in R1 as depicted above, and they have no obvious difference in orientations from the surrounding deformed matrix due to inadequate time to adjust their orientations. Further, {111} grains account for a large proportion at the center layer of the cold-rolled sample [13], and thus, the γ-fiber dominates the texture at this stage. Nuclei generated from sub-grains in R3 are thermodynamically unstable and tend to adjust their orientations favorably to grow when they happen to encounter non-uniformly distributed energy in a {111} matrix or {111}–{100} boundaries upon HTA-60, which is associated with growth selection [21, 22], leading to the occurrence of randomly oriented grains. Therefore, grains with random orientations account for a large portion at this stage. Compared to R3, more thermodynamically stable nuclei exist in R4 and R5, with less surrounding stored energy in the matrix. In particular, R5 even shows a small increase in the γ-fiber and a certain decrease in both the θ-fiber and random orientations. In summary, pre-recovery before primary recrystallization can weaken the γ-fiber and strengthen the θ-fiber and random orientations, thus homogenizing the macro-texture. Further, sufficient recovery (LTA for 60 min) before recrystallization not only homogenizes the texture but also contributes to obtaining equiaxed and fine grains.

Conclusions

The effects of recovery on the subsequent recrystallization of Ta were investigated in this paper. Some conclusions can be drawn as follows.

(1) Controlling the degree of pre-recovery can regulate the fraction of nucleation mechanisms, including SG and HABM mechanisms, and can adjust nucleation behavior to optimize the recrystallization morphology.

(2) The main changes introduced by pre-recovery originated in the evolution of dislocation morphology. During recovery, submicron bands evolved into sub-grains and then rotated and coalesce into larger ones, accompanied by a more homogeneous distribution of dislocations. In particular, sub-grains formed upon pre-recovery tended to be equiaxed.

(3) Newly formed thermodynamically unstable nuclei can rotate further to grow more easily when they meet a high temperature. Thus, a 10-min recovery and a subsequent HT-60 process lead to the formation of many grains with relatively random orientations.

(4) Energy distribution is a function of pre-recovery time. Elongated grains formed along grain boundaries or in the interior of deformed grains mainly due to the heterogeneous distribution of stored energy. Meanwhile, grains tend to be equiaxed after a long recovery because of the uniform distribution of energy and the high density of nuclei formed during pre-recovery.

(5) Coarse grains and a strong texture were exhibited in the specimen without recovery before recrystallization, while equiaxed, fine grains and a uniformly distributed texture were found after long-time recovery and HT-60 treatment. Thus, an ample, thorough recovery before recrystallization can effectively homogenize the microstructure and texture of clock-rolled Ta.

Compliance with ethical standards

Conflict of interest We declare that we have no financial and personal relationships with other

people or organizations that can inappropriately influence our work; there is no professional or other personal interest of any nature or kind in any product, service and/or company that could be construed as influencing the position presented in, or the review of the manuscript entitled.

References

[1] Humphreys FJ, Hatherly M (2004) Recrystallization and related annealing phenomena, 2nd edn. Elsevier, Amsterdam

[2] Clausmeyer T, Gersein G, Bargmann S, Svendsen B, Van den Boogarrd AH, Zillmann B (2012) Experimental characterization of microstructure development during loading path changes in bcc sheet steels. J Mater Sci 48:674–689. doi:10.1007/s10853-012-6780-9

[3] Zhang Y, Wang JT, Cheng C, Liu JQ (2008) Stored energy and recrystallization temperature in high purity copper after equal channel angular pressing. J Mater Sci 43:7326–7330. doi:10.1007/s10853-008-2903-8

[4] Raabe D (2014) Recovery and recrystallization: phenomena, physics, models simulation. Phys Metall. doi:10.1016/b978-0-444-53770-6.00023-x

[5] Kazeminezhad M (2008) Relationship between the stored energy and indentation hardness of copper after compression test: models and measurements. J Mater Sci 43:3500–3504. doi:10.1007/s10853-008-2454-z

[6] Kuo C-M, Lin C-S (2007) Static recovery activation energy of pure copper at room temperature. Scripta Mater 57:667–670. doi:10.1016/j.scriptamat.2007.06.054

[7] Nes E (1995) Recovery revisited. Acta Metall Mater 43:2189–2207

[8] Bréchet YJM, Zurob HS, Hutchinson CR (2009) On the effect of pre-recovery on subsequent recrystallization. Int J Mater Res 100:1446–1448

[9] Liu WC, Li J, Yuan H, Yang QX (2007) Effect of recovery on the recrystallization texture of an Al–Mg alloy. Scripta Mater 57:833–836. doi:10.1016/j.scriptamat.2007.07.008)

[10] Srinivasan R, Viswanathan GB, Levit VI, Fraser HL (2009) Orientation effect on recovery and recrystallization of cold rolled niobium single crystals. Mater Sci Eng A 507:179–189. doi:10.1016/j.msea.2008.12.013

[11] Michaluk CA (2002) Correlating discrete orientation and grain size to the sputter deposition properties of tantalum. J Electron Mater 31:2–9

[12] Deng C, Liu SF, Hao XB, Ji JL, Zhang ZQ, Liu Q (2014) Orientation dependence of stored energy release and microstructure evolution in cold rolled tantalum. Int J Refract Metal Hard Mater 46:24–29. doi:10.1016/j.ijrmhm.2014.05.005

[13] Liu SF, Fan HY, Deng C, Hao XB, Guo Y, Liu Q (2015) Through-thickness texture in clock-rolled tantalum plate. Int J Refract Metal Hard Mater 48:194–200. doi:10.1016/j.ijrmhm.2014.08.019

[14] Kim DI, Kim JS, Kim JH, Choi SH (2014) A study on the annealing behavior of Cu-added bake-hardenable steel using an in situ EBSD technique. Acta Mater 68:9–18. doi:10.1016/j.actamat.2014.01.005

[15] Varma SK, Bardford C (1988) Wesstrom, Effect of cold work on subgrain growth during recovery in pure aluminium. J Mater Sci Lett 7:1092–1093

[16] Rez-Prado MTP, Hines JA, Vecchio KS (2001) Microstructural evolution in adiabatic shear bands in Ta and Ta–W alloys. Acta Mater 49:2905–2917

[17] Raabe D (1995) On the orientation dependence of static recovery in low-carbon steels. Scr Metall Mater 33:735–740

[18] Vandermeer RA, Snyder WB (1979) Recovery and recrystallization in rolled tantalum single crystals. Metall Trans A 10A:1031–1044

[19] Humphreys FJ (2004) Nucleation in recrystallization. Mater Sci Forum 467–470:107–116. doi:10.4028/www.scientific.net/MSF.467-470.107

[20] Gaitzsch U, Rodig C, Damm C, Schultz L (2015) Elongated grains in Ni5 W(Ag) RABiTS tapes. J Alloy Compd 623:132–135. doi:10.1016/j.jallcom.2014.10.098

[21] Raabe D, Schlenkert G, Weisshaupt H, LOcke K (1994) Texture and microstructure of rolled and annealed tantalum. Mater Sci Technol 10:299–305

[22] Sidor JJ, Petrov RH, Kestens LAI (2011) Modeling the crystallographic texture changes in aluminum alloys during recrystallization. Acta Mater 59:5735–5748. doi:10.1016/j.actamat.2011.05.050